Materials Chemistry and Physics 243 (2020) 122600

Contents lists available at ScienceDirect

Materials Chemistry and Physics

journal homepage: www.elsevier.com/locate/matchemphys

In situ polymerization of aniline on the surface of manganese oxide nanosheets for reducing fire hazards of epoxy

Dengdeng Xie [a], Youming Han [a], Keqing Zhou [a,*], Congling Shi [b,**]

[a] Faculty of Engineering, China University of Geosciences (Wuhan), Wuhan, Hubei, 430074, PR China
[b] Beijing Key Laboratory of Metro Fire and Passenger Transportation Safety, China Academy of Safety Science and Technology, Beijing, 100012, PR China

HIGHLIGHTS

- Binary hybrids (PANI-MnO_2 hybrids) were prepared by in-situ polymerization method.
- The PANI-MnO_2 hybrids exhibited a homogeneous dispersion in the epoxy matrix.
- The PANI-MnO_2 hybrids had positive effects on decrease of PHRR, THR and SPR.
- The PANI-MnO_2 hybrids promote the formation of compact char layer during combustion.

GRAPHICAL ABSTRACT

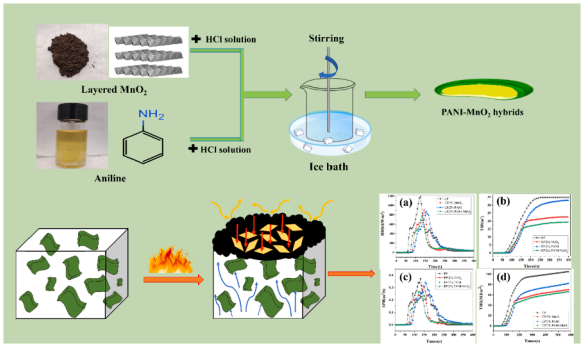

ARTICLE INFO

Keywords:
MnO_2 nanosheets
Dispersibility
Interfacial interaction
Fire safety
Epoxy

ABSTRACT

Layered manganese dioxide (MnO_2) is a promising nanofillers for reducing the fire hazards of polymeric materials due to its excellent catalytic charring effect. However, its poor dispersion in polymer matrices hindered its full performance. In this work, polyaniline (PANI) coatings were uniformly coated on the surface of MnO_2 nanosheets by in-situ polymerization method to form binary hybrids (PANI-MnO_2 hybrids). The prepared PANI-MnO_2 hybrids were characterized by X-ray diffraction (XRD), Fourier transform infrared (FTIR), Thermogravimetric analysis (TGA), X-ray photoelectron spectroscopy (XPS) and Scanning electron microscopy (SEM). SEM results of the fractured surface indicated the dispersibility and interfacial interaction between MnO_2 and epoxy (EP) matrix were obviously improved, leading to superior fire safety performance of epoxy-based composites. By adding 2 wt% of PANI-MnO_2 hybrids, the peak heat release rate (PHRR), total heat release (THR), total smoke production (TSP) and peak smoke production rate (PSPR) values of EP composites were decreased by 34.7%, 37.1%, 44.4%, and 27.0% respectively, compared to those of pure EP. The good dispersion and interfacial interaction of PANI-MnO_2 hybrids and the catalysis and physical barrier of MnO_2 nanosheets contributed to the superior fire safety performance of EP composites.

* Corresponding author.
** Corresponding author.
E-mail addresses: zhoukq@cug.edu.cn (K. Zhou), shicl@chinasafety.ac.cn (C. Shi).

https://doi.org/10.1016/j.matchemphys.2019.122600
Received 29 October 2019; Received in revised form 30 November 2019; Accepted 30 December 2019
Available online 31 December 2019

1. Introduction

Epoxy resin (EP) is an indispensable polymer in modern production and life. It has been widely used in many fields due to its high mechanical properties, excellent chemical resistance and insulation [1–3]. However, fires have become a demon that limits the normal use of many polymeric materials. Due to the high flammability of epoxy, the limiting oxygen index is only 19, which inevitably leads to fire and seriously affects its safe use [4]. As we all know, a lot of heat and smoke were generated when EP was burned, which were the two major causes of death in fires accidents [5]. Therefore, reducing the release of heat and smoke during the combustion of EP resin is particularly important.

At present, various layered nanofillers including graphene [6,7], layered double hydroxide [8,9], molybdenum disulfide [10], etc. had been adopted to boost the fire safety of polymer materials due to the "tortuous path" effect of nanosheets, which effectively delayed heat release and pyrolysis products diffusion [11]. Due to its natural richness, low cost and easy availability, environmental friendliness and wide structural diversity and unique physicochemical properties, MnO_2 has been widely used in the fields of electrode materials [12,13] and catalyst [14,15]. Meanwhile, it's well known that catalytic carbonization is very significant to improve the flame retardancy of materials [16]. As a physical barrier, the carbon layer can delay the escape of pyrolysis gases and penetration of heat and mass transfer. Obviously, the catalytic activity of MnO_2 can increase the char forming ability of polymer during thermal degradation process. Moreover, some studies have shown that MnO_2 has potentials in inhibiting the release of heat and smoke during combustion [17,18]. Nevertheless, similar to the other nanomaterials, the dispersion of MnO_2 and interfacial interaction between MnO_2 and polymer matrices were poor, which will limit the improvements of performances. Thus, it's highly desirable to solve these two issues by modifying the surface characteristics of MnO_2.

Polyaniline (PANI) is a very attractive conductive polymer with a wide range of applications in supercapacitors [19,20], lithium-ion batteries [21] and electromagnetic shielding [22]. In addition, recent researches have shown that the introduction of PANI can reduce the fire hazards of composites, primarily attributing to the char forming ability of conjugated PANI [11]. Furthermore, a covalent bond will be formed between the amine groups in the structure of PANI molecule and EP chains, which is conducive to improve the interfacial interaction. Some studies had also confirmed that PANI can significantly enhance the dispersion properties and interfacial interaction of nanofillers in epoxy matrix [23,24]. Interestingly, PANI coating can be formed on nanoparticles by in-situ polymerization method, which provides a probability that PANI and MnO_2 could combine with each other tightly. It's expected that by coating PANI on the surface of MnO_2 will improve its dispersibility and enhance the interfacial interaction of the hybrids in the EP matrices, thereby solving the defect of poor dispersion of MnO_2 in EP matrix and reducing the fire hazards of EP composites ultimately.

In present work, the functionalized PANI-MnO_2 hybrids were constructed by in-situ polymerization of aniline monomer on the surface of MnO_2 nanosheets. The fabricated PANI-MnO_2 hybrids were characterized by XRD, FTIR, TGA, XPS, SEM and further incorporated into EP matrix. Finally, the influences of PANI-MnO_2 hybrids on the thermal and fire behaviors of EP composites were investigated and the char residues after combustion test was analyzed.

2. Materials and experimental

2.1. Materials

Potassium permanganate ($KMnO_4$), hydrochloric acid (HCl), ethyl acetate, aniline, ammonium persulfate (APS), 4, 4-diamino-diphenylmethane (DDM) and acetone were bought from Sinopharm Chemical Reagent Co., Ltd. (China). EP was provided by Hefei Jiangfeng Chemical Co., Ltd.

2.2. Synthesis of PANI-MnO_2 hybrids

1.422 g $KMnO_4$ was added into a three-necked flask, and then 140 mL of ethyl acetate and 450 mL of deionized water were incorporated. The above solutions were mixed together and sonicated for 30 min

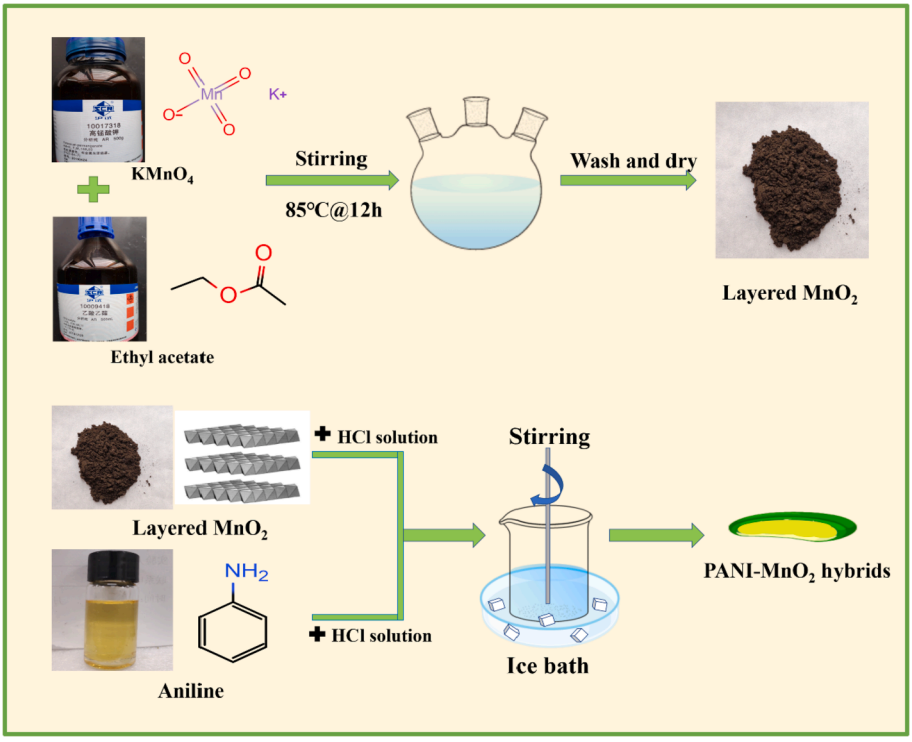

Scheme 1. Process for the fabrication of PANI-MnO_2 hybrids.

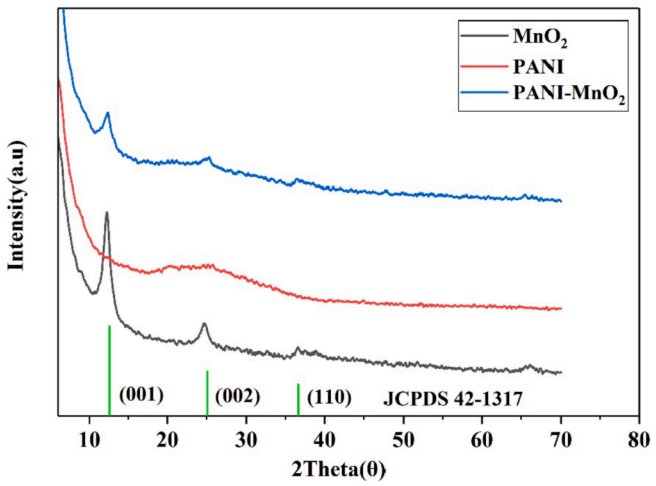

Fig. 1. XRD patterns of MnO_2, PANI and PANI-MnO_2 hybrids.

under stirring. Next, the solution was heated to 85 °C and held until the disappearance of pink color of $KMnO_4$. Thereafter, the resulting solution was centrifuged at 5000 rpm, followed by washing with deionized water and ethanol for several times, then dried at 80 °C for 24 h.

The PANI-MnO_2 hybrids was prepared by in situ polymerization method, the preparation route was shown in Scheme 1. 0.4 g of the pre-prepared MnO_2 was dispersed in 150 mL HCl aqueous solution (0.02 M) and stirred under ultrasonication in an ice bath. The aniline monomer (500 μL) was introduced into a beaker containing 100 mL of aqueous HCl (0.02 M) and kept in the ice bath for half an hour. Then, the abovementioned two solutions were quickly mixed and stirred for 10 h in an ice bath. The precipitates were centrifuged at 4500 rpm, and the obtained products were washed several times with deionized water and then dried overnight in an oven at 60 °C. Virgin PANI was prepared under the similar procedure, but APS was incorporated into the aniline solution as initiator to aid polymerization.

2.3. Preparation of EP based composites

Firstly, 1.2 g of PANI-MnO_2 hybrids were dispersed into 60 mL acetone and sonicated for 2 h to get a homogeneous solution. Next, EP was preheated at 80 °C to lower its viscosity, and then 60.0 g of EP was mixed into the prepared dispersion under high-speed mechanical stirring, and sonication was continued for several hours. Then, the mixture was transferred to an oil bath at 80 °C and heated overnight to completely evaporate the acetone. After that, 12.0 g of DDM was melted at 120 °C and dripped into the mixture and mechanically stirred for a few minutes. Finally, the preparation of EP composites was completed after the mixture pre-cured at 100 °C for 2 h and then post-cured at 150 °C for 2 h. The pure EP and EP composites with PANI and MnO_2 were also prepared through a similar procedure.

2.4. Characterization

X-ray diffraction (XRD, Germany Bruker AXS D8-Focus) was performed on a Cu- Kα tube and a Ni filter (λ = 0.154 nm). Fourier transform infrared (FTIR) spectra were accomplished by a Nicolet is50 spectrometer (Nicolet Instrument Corporation, Madison, WI). X-ray photoelectron spectroscopy (XPS) was recorded by VGESCALB MK-II electron spectrometer with Al Kα excitation source at 1486.6 eV. Thermogravimetric analysis (TGA) was performed by using a STA 409 PC Luxx simultaneous thermal analyzer (NETZSCH, Bavaria, Germany). Combustion test was characterized by a cone calorimeter (Fire Testing Technology, UK, heat flux of 35 kW/m^2) according to ISO 5660 standard. Scanning electron microscopy (SEM, SU-8010, Japan Hitachi Co, Ltd) was employed to detect the morphology of the fractured sections of EP composites and char residues after combustion test. An energy dispersive spectrometer (SEM-EDS) was also adopted to record the elemental composition and mapping.

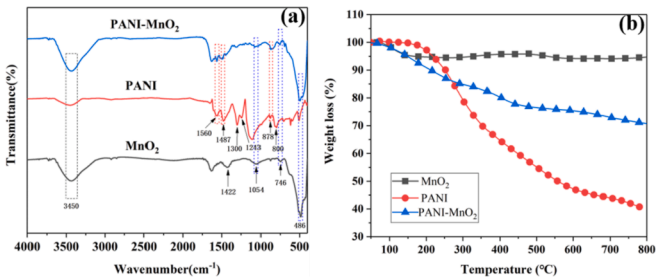

Fig. 2. (a) FTIR spectra and (b) TGA curves of MnO_2, PANI and PANI-MnO_2 hybrids.

3. Results and discussion

3.1. Characterization of PANI-MnO_2 hybrids

The MnO_2, PANI and PANI-MnO_2 hybrids were analyzed by XRD to confirm the successful modification of MnO_2 (Fig. 1). As for the MnO_2, the main diffraction peaks appeared at approximately 12.3°, 25°, and 36.4°, corresponding to the (001), (002) and (110) planes of MnO_2, respectively, which was in consistence with JCPDS card (No. 42-1317) [25,26]. On the curve of PANI, the peaks located at approximately 20° and 25° were corresponded to the (020), (200) planes of PANI, respectively [27,28]. For the prepared PANI-MnO_2 hybrids, the major diffraction peaks were almost identical to those of MnO_2 and PANI. However, the peak intensities were lower, which probably due to the presence of uniform PANI coating on the surface of MnO_2 nanosheets. The XRD analysis results suggested that the surface of MnO_2 nanosheets had been successfully wrapped by PANI.

FTIR spectra and TGA were further employed to prove the successful fabrication of PANI-MnO_2 hybrids. Fig. 2a shows the FTIR absorption spectrum of the MnO_2, PANI and PANI-MnO_2. In the FTIR spectra, the characteristic absorption peaks of all three samples located around 3450 cm^{-1} were mainly due to the stretching and bending vibrations of water molecules and hydroxyl groups [29,30]. For the MnO_2, the peaks appeared around 1422 and 746 cm^{-1} were attributed to the vibrations of the O–Mn–O bond of MnO_2 [31–33]. The absorption bands at 1054 and 486 cm^{-1} were possibly assigned to Mn^{3+}-O vibration and Mn–O vibrations in MnO_6 octahedral [33], respectively. The above results indicated that MnO_2 was successfully synthesized. As for pure PANI, the strong absorption band at 1560 cm^{-1} was attributed to the quinonoid structure of PANI, while the other sharp band at 1487 cm^{-1} was assigned to the benzenoid structure of PANI [34,35]. The stretching bands at 1300 and 1243 cm^{-1} were related to the C–N and C–N^+ stretching vibrations of the benzenoid units in PANI, respectively [36]. The appearance of bands at 878 and 800 cm^{-1} was the evidence for the C–H out of plane bending vibration of quinoid and benzenoid rings, respectively [36–38]. These characteristic bands prove that PANI had been successfully prepared. Moreover, characteristic adsorption bands of PANI and MnO_2 were also detected in the FTIR spectrum of PANI-MnO_2 hybrids, such as the peaks of 1562, 1483 and 874 cm^{-1} corresponding to PANI, and the peaks of 1071, 755 and 494 cm^{-1} attributing to MnO_2. The FTIR analysis results demonstrated that PANI coatings were decorated on the surface of MnO_2 nanosheets.

Fig. 2b presented the TGA results of MnO_2, PANI and PANI-MnO_2 hybrids. It can be observed that the weight loss of MnO_2 was very small (only 5.3%) during thermal degradation process under nitrogen atmosphere, which was mainly caused by the mass loss of interlayer water molecules. In contrast, the weight loss of PANI at 800 °C was 60.2%,

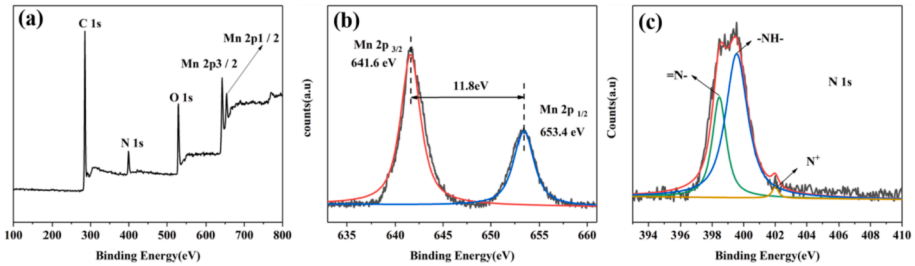

Fig. 3. XPS spectra of PANI-MnO_2 hybrids (a), high-resolution XPS spectra of Mn 2p (b) and N 1s (c) peaks.

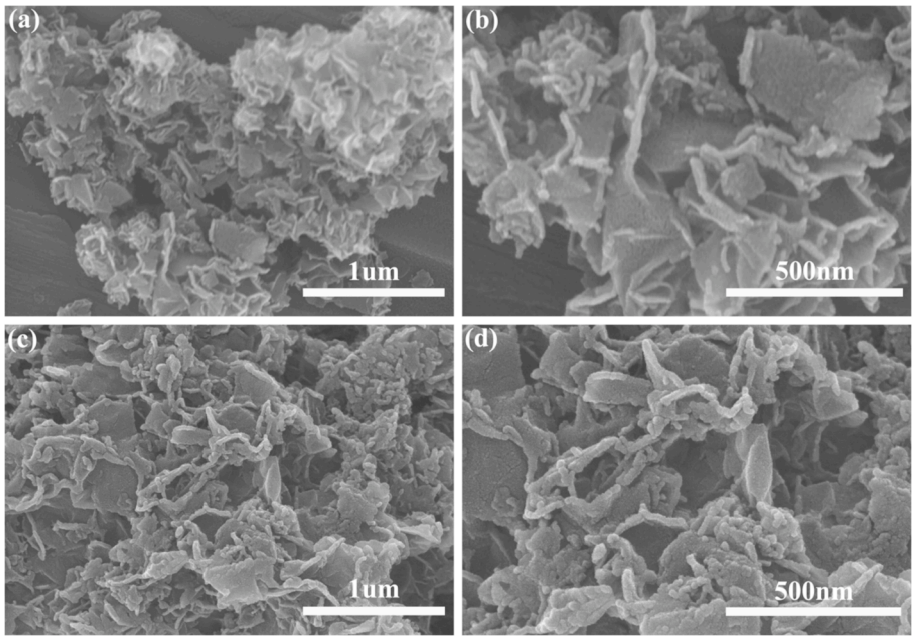

Fig. 4. SEM images of (a, b) MnO_2 and (c, d) PANI-MnO_2 hybrids.

corresponding to the large-scale degradation of PANI. As for the PANI-MnO_2 hybrids, the weight loss at 800 °C was 29.3%. Based on the weight loss of MnO_2, PANI and PANI-MnO_2 hybrids, the content of PANI coating decorated on the surface of MnO_2 nanosheets was calculated to be about 43.7 wt%, indicating that the surface was highly modified. The high quality PANI coating will provide a "bridge connection" role for the good auxiliary dispersion of MnO_2 nanosheets in EP matrices.

The XPS full scan-survey spectra and high-resolution spectra of PANI-MnO_2 hybrids were clearly exhibited in Fig. 3. In the full scan-survey spectra of the hybrids (Fig. 3a), the C, N, O, and Mn elements were detected. Fig. 3b exhibited the high-resolution spectral characteristic of Mn 2p in the hybrids. The peaks located at 653.4 and 641.6 eV with a spin–orbital splitting of 11.8 eV were corresponded to Mn 2p 1/2 and Mn 2p 3/2, respectively, which proved that MnO_2 was contained in

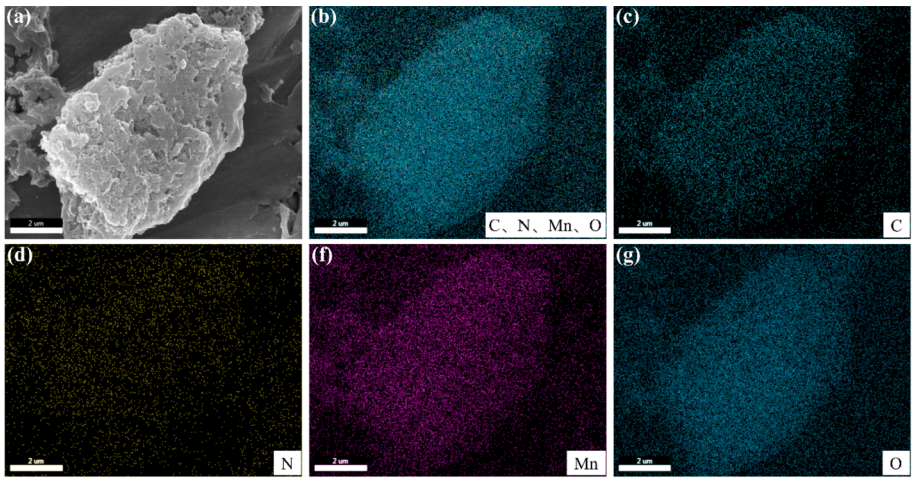

Fig. 5. Elemental mappings analysis results of PANI-MnO_2 hybrids.

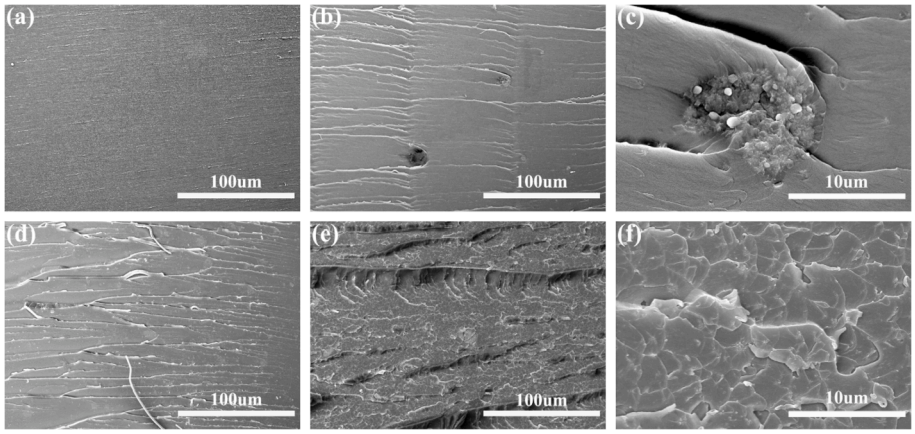

Fig. 6. SEM images of fracture surface of EP and its composites: (a) EP, (b, c) EP/MnO_2, (d) EP/PANI, (e, f) EP/PANI-MnO_2.

the hybrids [39,40]. The N 1s spectra of PANI-MnO_2 hybrids can be deconvoluted into three components at 398.45 eV, 399.55 eV, and 402 eV, which was attributed to the undoped imine (=N-), undoped amine (-NH-) and the protonated nitrogen (N^+), respectively [41]. These analyses strongly indicated the co-existence of PANI and MnO_2 in the prepared hybrids.

SEM was used to characterize the micro morphologies of the obtained samples. The SEM images of MnO_2 and PANI-MnO_2 hybrids were given in Fig. 4. As shown in Fig. 4a and b, MnO_2 was composed of many nanoflakes [42]. After the wrapping of PANI shell, the hybrids still presented a 2D lamellar structure at the same magnification, but the surface becomes rough and fuzzy, a "villi" granular material appeared and the flaky morphology obviously became thicker (Fig. 4c and d). This further confirmed that the PANI-MnO_2 hybrids had been successfully prepared. In order to further analyze the elemental composition of PANI-MnO_2 hybrids clearly, SEM element mapping was used to reveal the spatial distribution of C, N, Mn and O elements in the hybrids (Fig. 5). As shown in Fig. 5, the distribution regions of C, N, Mn and O elements were consistent with the position of the sample, and matched well with its outline. This also proved that PANI was uniformly covered on the surface of MnO_2 nanosheets.

3.2. Dispersibility

Generally, the dispersion status and interfacial interaction between the nanofillers and polymer matrices was critical to the performance of composites. Therefore, it was necessary to evaluate the dispersibility of the nanofillers and its interfacial interaction with polymer matrix. Fig. 6 displayed the fracture surfaces of EP and EP composites, respectively. As for pure EP (Fig. 6a), the micro-morphology of the fracture surfaces was smooth and featureless, indicated the brittleness of thermosetting polymer [43]. The fracture surface of the EP/PANI (Fig. 6d) had a pull filamentous pattern and had a broken filament on the surface, which indicated good interfacial interactions were formed between PANI and EP matrix. This might be due to the presence of active amine groups in PANI, which could participate in the curing reaction of epoxy and form chemical bonds with epoxy molecules [11]. By contrast, the fracture surface of EP/MnO_2 composites had slight texture, the surface was slightly rougher than that of pure EP, and visible dot-like agglomerates appeared. The presence of the agglomerates was probably due to the poor compatibility and interfacial interaction between MnO_2 nanosheets and EP matrix. However, the PANI-MnO_2 hybrids dispersed well in EP composites without no obvious agglomerates. The appearance of rough surface indicated the formation of good interfacial interaction between the hybrids and EP matrices. Additionally, this phenomenon also indicated that PANI could act as a "bridge" to promote the dispersion of MnO_2 nanosheets and improve its interface interaction with the matrices.

3.3. Thermal and fire behavior

3.3.1. Thermal stability

According to previous studies [44], the overall thermal stability of polymer material had a certain impact on its flame retardancy. Thus, the thermal degradation behavior of EP and its composites was studied by TGA. Fig. 7 showed the TGA and DTG curves of EP and its composites, and the related data of TGA were presented in Table 1. Noteworthily, all samples had similar thermal decomposition behavior, indicating that

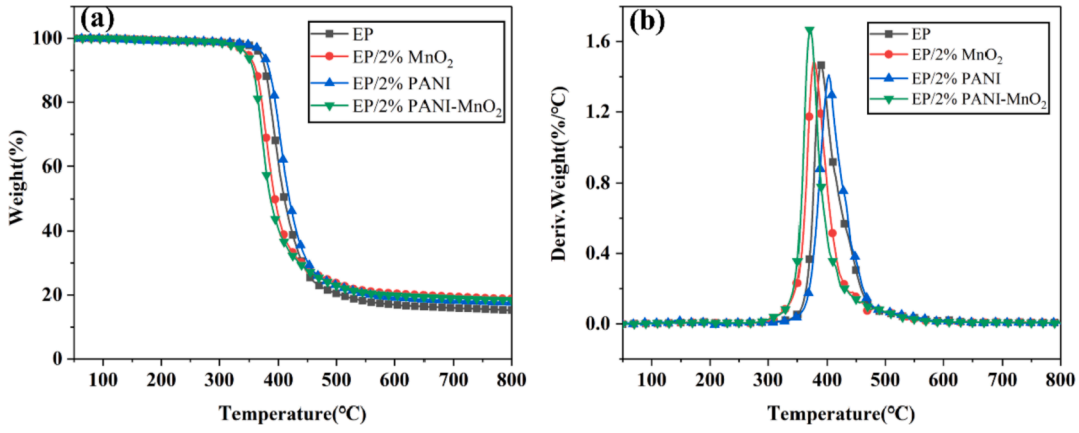

Fig. 7. TGA (a) and DTG (b) curves of EP and its composites.

Table 1
Related TGA data of EP and its composites.

Sample	$T_{initial}$ (°C)	T_{max} (°C)	Char yield (%)
EP	369	390	15.2
EP/2%MnO_2	348	378	18.7
EP/2%PANI	374	403	17.6
EP/2%PANI- MnO_2	346	370	18.5

the introduction of nanofillers did not affect the decomposition mechanism of EP. As can be seen from the DTG curves, there were only one sharp stage of weightlessness for all samples, mainly because of the degradation of EP networks. Generally, the temperature at which the weight loss is 5 wt% is defined as the initial degradation temperature ($T_{initial}$) and the maximum decomposition temperature (T_{max}) corresponded to the point at the maximum decomposition rate of the DTG curves. In addition to EP/PANI composites, the $T_{initial}$ and T_{max} of other EP composites are lower than those of pure EP. This might be due to the catalytic effect of MnO_2 on the EP resin, which led to accelerated pyrolysis and carbonization of the polymer. However, in terms of char residues, all EP composites had higher amounts of char yield than pure EP. It was observed that EP composites containing MnO_2 (EP/MnO_2 and EP/PANI-MnO_2) could provide a higher amount of char yield, compared with EP (15.2%) and EP/PANI (17.6%) composites. Therefore, the addition of MnO_2-based nanofillers could effectively promote the formation of char layer during thermal degradation process, which could help reduce flammable gas release and hinder oxygen exchange and energy transfer.

3.3.2. *Fire safety*

Cone calorimeter was commonly employed to assess the combustion behavior of various materials [45]. The fire performances of the materials were evaluated by parameters including heat release rate (HRR), total heat release (THR), smoke production rate (SPR), and total smoke production (TSP). The HRR, THR, SPR and TSP curves for EP and its composites and the corresponding data were listed in Fig. 8 and Table 2. As for pure EP, it exhibited a distinct HRR curve with a peak heat release rate (PHRR) of 1183.0 kW/m^2 and a THR of 104.9 MJ/m^2. After the inclusion of nanofillers, the heat release of the composites was inhibited at varying degrees. The introduction of PANI nanofillers led to the reduction of HRR, the PHRR value of EP/PANI composites was 867.7 kW/m^2. The PANI as a nitrogen-containing compound, its amine group had a certain flame retardant effect and helped to reduce HRR [46]. By mixing 2 wt% of MnO_2 into EP matrix, its PHRR value was 901.5 kW/m^2, lower than that of pure EP. However, the combustion of the EP composites containing PANI-MnO_2 hybrid was significantly suppressed. The PHRR value of EP/PANI-MnO_2 composites dropped to 772.1 kW/m^2, corresponding to a 34.7% reduction compared to pure EP. In addition, the introduction of PANI-MnO_2 hybrids also caused a significant decrease in THR value compared to pure EP, which was decreased by 37.1%. It was obvious that the presence of polyaniline coating can increase the flame retardant efficiency of MnO_2.

As is known to all, the main cause of death in fires is the generation of smoke particles and some toxic gases [47]. The SPR and TSP curves for pure EP and EP composites were displayed in Fig. 8c and d. In the SPR

Table 2
Related cone calorimeter results of pure EP and its composites.

	EP	EP/2% MnO_2	EP/2% PANI	EP/2% PANI- MnO_2
PHRR(kW/m^2)	1183.0	901.5	867.7	772.1
THR(MJ/m^2)	104.9	70.2	82.0	66.0
TSP(m^2)	34.9	22.7	33.1	19.4
PSPR(m^2/s)	0.37	0.31	0.34	0.27
Char yield (%)	17.9	31.7	26.6	34.3

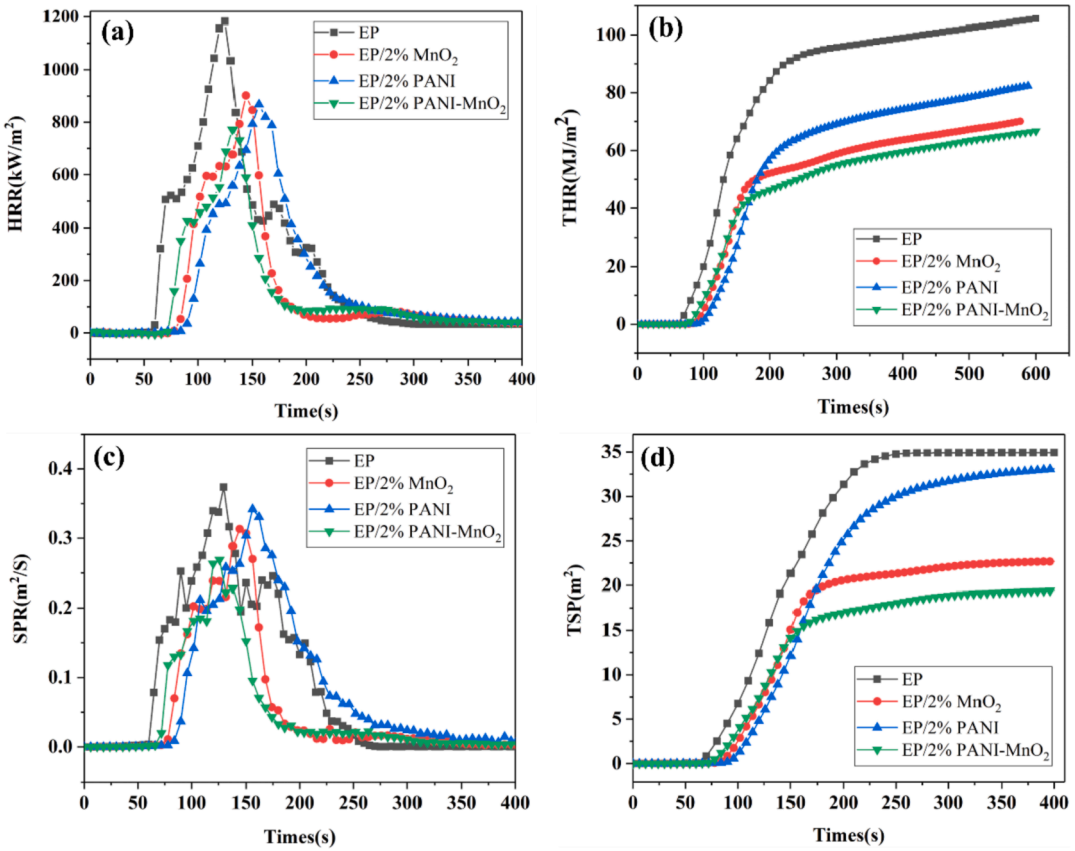

Fig. 8. (a) HRR, (b) THR, (c) SPR (d) TSP curves of EP and EP composites.

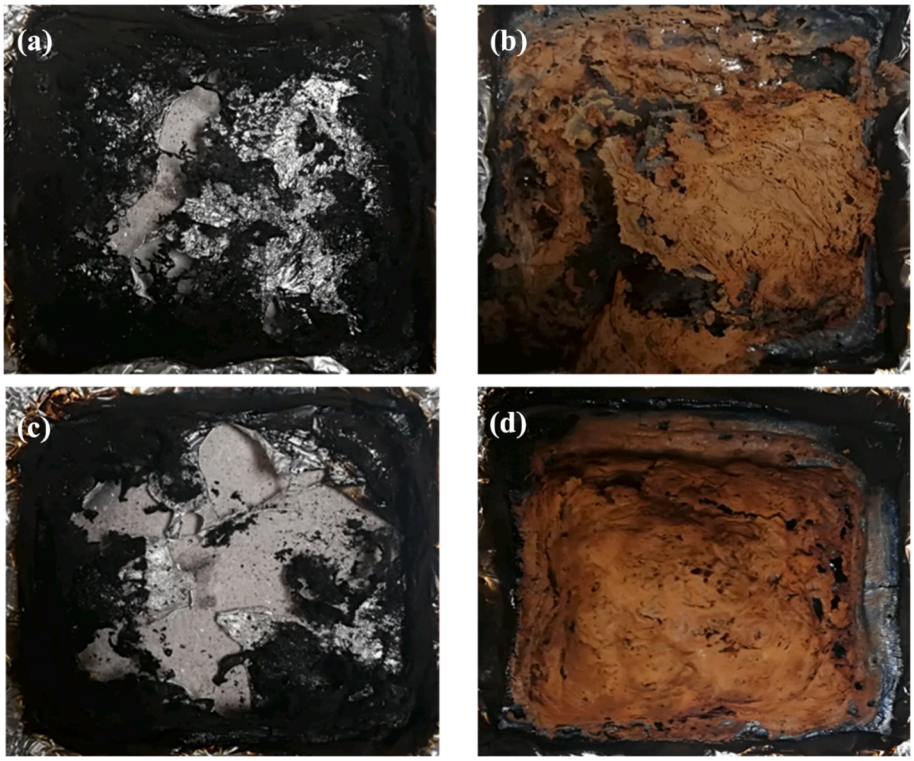

Fig. 9. Digital photos of the char residues of EP (a), EP/MnO_2 (b), EP/PANI (c) and EP/PANI-MnO_2 (d) after combustion test.

curve, both the PSPR values and the smoke release time after the addition of the nanofillers were smaller than those of pure EP. Among them, the PSPR of EP/MnO_2, EP/PANI, EP/PANI-MnO_2 composites decreased from 0.37 m^2/s of neat EP to 0.31, 0.34 and 0.27 m^2/s, respectively, and the composites with PANI-MnO_2 hybrids had the most obvious decline effect, which was 27% lower than pure EP. Furthermore, the EP/PANI-MnO_2 composites had the lowest TSP, which was 44.4% lower than pure EP and 14.5% lower than EP/MnO_2 composites. These results fully demonstrated that PANI-MnO_2 hybrids had excellent smoke suppression function on EP during combustion.

3.3.3. Char residues analysis

The char yield was one of the key parameters for evaluating the combustion performance of composite materials [48]. From the cone calorimetric data in Table 2, the char yield of EP/MnO_2, EP/PANI and EP/PANI-MnO_2 composites were 31.7%, 26.6% and 34.3%, respectively, under the same loading conditions. The EP/PANI-MnO_2 composites has the highest char yield, which was 92% higher than pure EP, and also 8.2% higher than EP/MnO_2 composites, indicating its excellent catalytic char forming ability.

The structure of the carbon layer formed after combustion was also

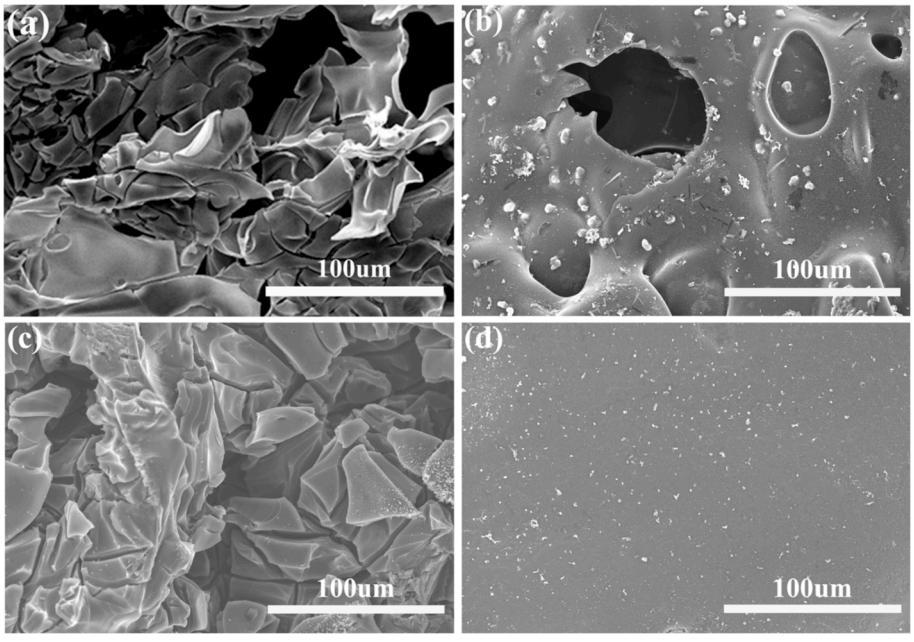

Fig. 10. SEM images of char residues of (a) EP, (b) EP/MnO_2, (c) EP/PANI and (d) EP/PANI-MnO_2.

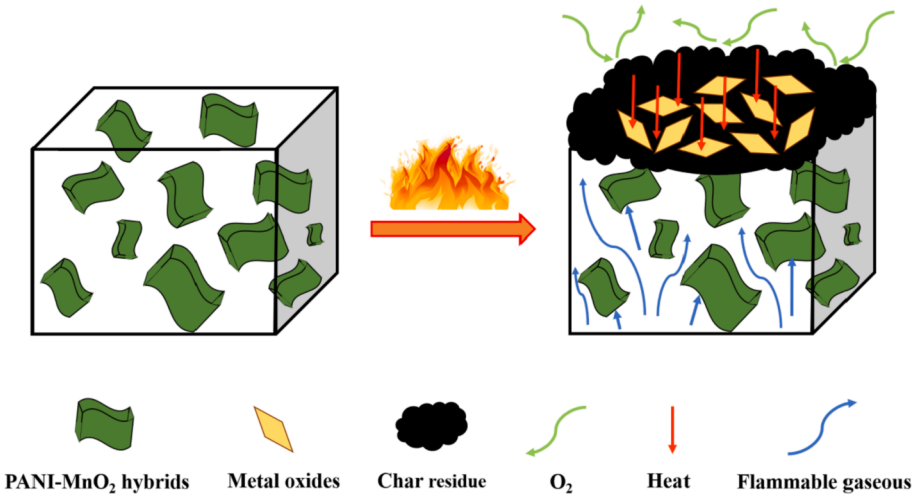

Scheme 2. Schematic illustration for flame retardant mechanism of EP composites containing PANI-MnO_2 hybrids.

an important factor affecting the flame retardancy [49]. Fig. 9 showed the digital photographs of char residues of EP and EP composites. As for pure EP, few char residues with sparse and fragile structure remained after combustion test (Fig. 9a). The amount of carbon residues in EP/PANI composites was higher than that of pure EP. Meanwhile, small lumpy carbon layers were observed at the edge, but it was discontinuous and only exist at the edges (Fig. 9c). The EP/MnO_2 composites had a large amount of char residues, and a yellow-brown "bread" arch appeared on the dense carbon layer (Fig. 9b), but the continuity of the carbon layer was poor, and the barrier performance could not be well exhibited. However, EP/PANI-MnO_2 composites exhibited a denser and continuous yellow-brown "bread" carbon layer morphology (Fig. 9d). According to previous reports [17], MnO_2 was conducive to the formation of a denser carbon layer, which could act as a thermal barrier against heat, oxygen and pyrolysis products. In addition, since the hybrids encapsulated by PANI had good dispersibility, the carbon layer formed after combustion was more continuous and compact, and the flame retarding effect in the condensed phase could be effectively exerted, thereby reducing the fire risk of polymer.

In order to reveal the flame-retardant mechanism, the surface micromorphology of the char residues was observed by SEM, and the results were shown in Fig. 10. In Fig. 10a, the char residues of pure EP were loose and porous, resulting in a thin and fragile irregular carbon layer, leaving a large number of pores and cracks. For the EP/PANI composites, an irregular bulk porous carbon layer appeared, but with low continuity (Fig. 10c). As for the EP/MnO_2 composites, it formed a dense and relatively continuous carbon layer structure, the only regret was that there were a large number of pores in the carbon layer. Surprisingly, after being wrapped by PANI, the EP/PANI-MnO_2 composites exhibited a complete and dense continuous carbon layer, and no holes were found (Fig. 10d), which demonstrated the excellent char forming ability of the PANI-MnO_2 hybrids. There may be attributed to the following two main reasons: (1) MnO_2 has excellent char forming effect and combines with the partial char forming ability of PANI; (2) the well dispersion and good interfacial adhesion of hybrids in EP matrix facilitate the formation of a uniform and dense char layer.

In summary, the introduction of PANI-MnO_2 hybrids greatly reduced the fire hazards of EP composites. Based on the above analysis, the flame retardancy mechanism was summarized, as shown in Scheme 2. Firstly, the dispersion and interfacial interaction of PANI-MnO_2 hybrids in EP matrix were improved by in-situ polymerization of PANI on the surface of MnO_2. Secondly, MnO_2 had good catalytic and carbonization ability, promoted the formation of dense carbon layers and reduced the release of toxic gases. In addition, the MnO_2 nanosheets had lamellar structure and the compact layered structures contributed to good physical barrier effect, thereby improving the flame retardancy of polymer materials.

4. Conclusion

In present work, functionalized PANI-MnO_2 hybrids were constructed by in-situ polymerization of aniline monomer on the surface of MnO_2 nanosheets. The hybrids were characterized by XRD, FTIR, TGA, XPS and SEM. The introduction of PANI coating significantly enhanced the dispersion and interfacial interaction of hybrids in EP matrix, thereby improving the overall fire safety of EP composites. By introducing 2 wt% PANI-MnO_2 hybrids into EP matrix, the PHRR and THR values were significantly reduced. Moreover, the values of TSP and PSPR were also significantly decreased, indicating an obvious decrease of the fire smoke toxicity. Overall, the addition of PANI-MnO_2 hybrids endowed excellent fire safety to EP composites. Good dispersibility and interfacial interaction of PANI-MnO_2 hybrids in EP matrix promoted the full release of the MnO_2 catalytic ability, forming a denser carbon layer, and layered MnO_2 could also act as a physical barrier to reduce the release of smoke and heat and improve the fire safety of polymer materials.

Declaration of competing interest

The authors declare no competing financial interest and conflict of interest form.

Acknowledgments

This work was supported by the Fundamental ResearchFundsfor theCentralUniversities, China University of Geosciences (Beijing) (Wuhan) (CUG160607), Natural Science Fund of Hubei Province (No. 2017CFB315), Opening Project of Engineering Research Center of Rock-Soil Drilling & Excavation and Protection, (China University of Geosciences (Beijing) (Wuhan), Ministry of Education (201801).

References

[1] N. Domun, H. Hadavinia, T. Zhang, et al., Improving the fracture toughness and the strength of epoxy using nanomaterials–a review of the current status, Nanoscale 7 (23) (2015) 10294–10329.
[2] K. Zhou, G. Tang, R. Gao, et al., In situ growth of 0D silica nanospheres on 2D molybdenum disulfide nanosheets: towards reducing fire hazards of epoxy resin, J. Hazard Mater. 344 (2018) 1078–1089.
[3] F. Jin, X. Li, S. Park, Synthesis and application of epoxy resins: a review, J. Ind. Eng. Chem. 29 (2015) 1–11.
[4] S. Wang, S. Ma, C. Xu, et al., Vanillin-derived high-performance flame retardant epoxy resins: facile synthesis and properties, Macromolecules 50 (5) (2017) 1892–1901.

[5] S. Zhao, J. Yin, K. Zhou, Y. Cheng, B. Yu, In situ fabrication of molybdenum disulfide based nanohybrids for reducing fire hazards of epoxy, Composites Part A 122 (2019) 77–84.

[6] B. Yu, Y. Shi, B. Yuan, et al., Enhanced thermal and flame retardant properties of flame-retardant-wrapped graphene/epoxy resin nanocomposites, J. Mater. Chem. 3 (15) (2015) 834–844.

[7] Y. Feng, C. He, Y. Wen, et al., Improving thermal and flame retardant properties of epoxy resin by functionalized graphene containing phosphorous, nitrogen and silicon elements, Compos. Appl. Sci. Manuf. 103 (2017) 74–83.

[8] E.N. Kalali, X. Wang, D. Wang, Functionalized layered double hydroxide-based epoxy nanocomposites with improved flame retardancy and mechanical properties, J. Mater. Chem. 3 (13) (2015) 6819–6826.

[9] K. Zhou, R. Gao, X. Qian, Self-assembly of exfoliated molybdenum disulfide (MoS_2) nanosheets and layered double hydroxide (LDH): towards reducing fire hazards of epoxy, J. Hazard Mater. 338 (2017) 343–355.

[10] R. Gao, S.G. Wang, K.Q. Zhou, X.D. Qian, Mussel-inspired decoration of $Ni(OH)_2$ nanosheets on 2D MoS_2 towards enhancing thermal and flame retardancy properties of poly(lactic acid), Polym. Adv. Technol. 30 (4) (2019) 879–888.

[11] K. Zhou, C. Liu, R. Gao, Polyaniline: a novel bridge to reduce the fire hazards of epoxy composites, Compos. Appl. Sci. Manuf. 112 (2018) 432–443.

[12] F. Li, Y. Xing, M. Huang, et al., MnO_2 nanostructures with three-dimensional (3D) morphology replicated from diatoms for high-performance supercapacitors, J. Mater. Chem. 3 (15) (2015) 7855–7861.

[13] M. Huang, F. Li, F. Dong, et al., MnO_2-based nanostructures for high-performance supercapacitors, J. Mater. Chem. 3 (43) (2015) 21380–21423.

[14] M.M. Najafpour, G. Renger, M. Hołyńska, et al., Manganese compounds as water-oxidizing catalysts: from the natural water-oxidizing complex to nanosized manganese oxide structures, Chem. Rev. 116 (5) (2016) 2886–2936.

[15] S. Chen, J. Duan, A. Vasileff, et al., Size fractionation of two-dimensional sub-nanometer thin manganese dioxide crystals towards superior urea electrocatalytic conversion, Angew. Chem. 128 (11) (2016) 3868–3872.

[16] H. Yu, Z. Jiang, J.W. Gilman, et al., Promoting carbonization of polypropylene during combustion through synergistic catalysis of a trace of halogenated compounds and Ni_2O_3 for improving flame retardancy, Polymer 50 (26) (2009) 6252–6258.

[17] W. Wang, Y. Kan, K. Meow Liew, et al., Comparative investigation on combustion property and smoke toxicity of epoxy resin filled with α- and δ-MnO_2 nanosheets, Compos. Appl. Sci. Manuf. 107 (2018) 39–46.

[18] W. Wang, Y. Kan, B. Yu, et al., Synthesis of MnO_2 nanoparticles with different morphologies and application for improving the fire safety of epoxy, Compos. Appl. Sci. Manuf. 95 (2017) 173–182.

[19] A. Eftekhari, L. Li, Y. Yang, Polyaniline supercapacitors, J. Power Sources 347 (2017) 86–107.

[20] S.K. Simotwo, C. Delre, V. Kalra, Supercapacitor electrodes based on high-purity electrospun polyaniline and polyaniline-carbon nanotube nanofibers, ACS Appl. Mater. Interfaces 8 (33) (2016) 21261–21269.

[21] L. Yi, L. Liu, G. Guo, et al., Expanded graphite@SnO_2@ polyaniline composite with enhanced performance as anode materials for lithium ion batteries, Electrochim. Acta 240 (2017) 63–71.

[22] N. Joseph, J. Varghese, M.T. Sebastian, Self assembled polyaniline nanofibers with enhanced electromagnetic shielding properties, RSC Adv. 5 (26) (2015) 20459–20466.

[23] K. Jlassi, S. Chandran, M.A. Poothanari, et al., Clay/polyaniline hybrid through diazonium chemistry: conductive nanofiller with unusual effects on interfacial properties of epoxy nanocomposites, Langmuir 32 (14) (2016) 3514–3524.

[24] H. Gu, S. Tadakamalla, Y. Huang, et al., Polyaniline stabilized magnetite nanoparticle reinforced epoxy nanocomposites, ACS Appl. Mater. Interfaces 4 (10) (2012) 5613–5624.

[25] M.H. Alfaruqi, J. Gim, S. Kim, et al., A layered δ-MnO_2 nanoflake cathode with high zinc-storage capacities for eco-friendly battery applications, Electrochem. Commun. 60 (2015) 121–125.

[26] T.T. Truong, Y. Liu, Y. Ren, et al., Morphological and crystalline evolution of nanostructured MnO_2 and its application in lithium-air batteries, ACS Nano 6 (9) (2012) 8067–8077.

[27] L. Ren, G. Zhang, Z. Yan, et al., Three-Dimensional tubular MoS_2/PANI hybrid electrode for high rate performance supercapacitor, ACS Appl. Mater. Interfaces 7 (51) (2015) 28294–28302.

[28] Y. Zhao, Z. Zhang, Y. Ren, et al., Vapor deposition polymerization of aniline on 3D hierarchical porous carbon with enhanced cycling stability as supercapacitor electrode, J. Power Sources 286 (2015) 1–9.

[29] M. Trchová, I. Aeděnková, J. Stejskal, In-situ polymerized polyaniline films 6. FTIR spectroscopic study of aniline polymerisation, Synth. Met. 154 (1–3) (2005) 1–4.

[30] L. Yang, Y. Zhu, G. Cheng, Synthesis of well-crystallized birnessite using ethylene glycol as a reducing reagent, Mater. Res. Bull. 42 (1) (2007) 159–164.

[31] Y. Huang, Y. Lin, W. Li, Controllable syntheses of α- and δ-MnO_2 as cathode catalysts for zinc-air battery, Electrochim. Acta 99 (2013) 161–165.

[32] Z. Ma, X. Wei, S. Xing, et al., Hydrothermal synthesis and characterization of surface-modified δ-MnO_2 with high Fenton-like catalytic activity, Catal. Commun. 67 (2015) 68–71.

[33] S. Maiti, A. Pramanik, S. Mahanty, Interconnected network of MnO_2 nanowires with a "Cocoonlike" morphology: redox couple-mediated performance enhancement in symmetric aqueous supercapacitor, ACS Appl. Mater. Interfaces 6 (13) (2014) 10754–10762.

[34] Y. Liu, Y. Ma, S. Guang, et al., Polyaniline-graphene composites with a three-dimensional array-based nanostructure for high-performance supercapacitors, Carbon 83 (2015) 79–89.

[35] J. Zhu, S. Wei, L. Zhang, et al., Polyaniline-tungsten oxide metacomposites with tunable electronic properties, J. Mater. Chem. 21 (2) (2011) 342–348.

[36] M. Trchová, J. Stejskal, J. Prokeš, Infrared spectroscopic study of solid-state protonation and oxidation of polyaniline, Synth. Met. 101 (1) (1999) 840–841.

[37] Y. Hayatgheib, B. Ramezanzadeh, P. Kardar, et al., A comparative study on fabrication of a highly effective corrosion protective system based on graphene oxide-polyaniline nanofibers/epoxy composite, Corros. Sci. 133 (2018) 358–373.

[38] A. Yelil Arasi, J. Juliet Latha Jeyakumari, B. Sundaresan, et al., The structural properties of Poly(aniline)—analysis via FTIR spectroscopy, Spectrochim. Acta A Mol. Biomol. Spectrosc. 74 (5) (2009) 1229–1234.

[39] M. Huang, X.L. Zhao, F. Li, et al., Synthesis of Co_3O_4/SnO_2@MnO_2 core-shell nanostructures for high-performance supercapacitors, J. Mater. Chem. 3 (24) (2015) 12852–12857.

[40] G. Wang, Q. Tang, H. Bao, et al., Synthesis of hierarchical sulfonated graphene/MnO_2/polyaniline ternary composite and its improved electrochemical performance, J. Power Sources 241 (2013) 231–238.

[41] D. Shao, G. Hou, J. Li, et al., PANI/GO as a super adsorbent for the selective adsorption of uranium (VI), Chem. Eng. J. 255 (2014) 604–612.

[42] Y. Zhang, C. Sun, P. Lu, et al., Crystallization design of MnO_2 towards better supercapacitance, CrystEngComm 14 (18) (2012) 5892.

[43] K.L. Gong, K.Q. Zhou, B. Yu, Superior thermal and fire safety performances of epoxy-based composites with phosphorus-doped cerium oxide nanosheets, Appl. Surf. Sci. (2019), https://doi.org/10.1016/j.apsusc.2019.144314.

[44] B.N. Jang, M. Costache, C.A. Wilkie, The relationship between thermal degradation behavior of polymer and the fire retardancy of polymer/clay nanocomposites, Polymer 46 (24) (2005) 10678–10687.

[45] S.G. Wang, R. Gao, K.Q. Zhou, The influence of cerium dioxide functionalized reduced graphene oxide on reducing fire hazards of thermoplastic polyurethane nanocomposites, J. Colloid Interface Sci. 536 (2019) 127–134.

[46] H. Horacek, R. Grabner, Advantages of flame retardants based on nitrogen compounds, Polym. Degrad. Stab. 54 (2) (1996) 205–215.

[47] K.Q. Zhou, R. Gao, Z. Gui, Y. Hu, The influence of graphene based smoke suppression agents on reduced fire hazards of polystyrene composites, Composites Part A 80 (2016) 217–227.

[48] D.T. Hu, Q.Q. Zhou, K.Q. Zhou, Combined effects of layered nanofillers and intumescent flame retardant on thermal and fire behavior of ABS resin, J. Appl. Polym. Sci. 136 (2019) 48220.

[49] B. Dittrich, K. Wartig, D. Hofmann, et al., Flame retardancy through carbon nanomaterials: carbon black, multiwall nanotubes, expanded graphite, multi-layer graphene and graphene in polypropylene, Polym. Degrad. Stab. 98 (8) (2013) 1495–1505.